Journal of Photochemistry and Photobiology A: Chemistry 251 (2013) 1–9

Contents lists available at SciVerse ScienceDirect

Journal of Photochemistry and Photobiology A: Chemistry

journal homepage: www.elsevier.com/locate/jphotochem

Tuning photophysical properties of triphenylamine and aromatic cyano conjugate-based wavelength-shifting compounds by manipulating intramolecular charge transfer strength

Yilin Li[a,b], Tianhui Ren[a,*], Wen-Ji Dong[b,**]

[a] School of Chemistry and Chemical Engineering, Shanghai Jiao Tong University, Shanghai 200240, China
[b] Voiland School of Chemical Engineering and Bioengineering, Washington State University, Pullman, WA 99164, USA

ARTICLE INFO

Article history:
Received 11 June 2012
Received in revised form 28 August 2012
Accepted 2 October 2012
Available online 17 October 2012

Keywords:
Triphenylamine
Wavelength-shifting materials
Large Stokes shift
ICT
DFT

ABSTRACT

A series of triphenylamine-based aromatic cyano compounds have been synthesized as red-emitting fluorophores with large Stokes shifts in both solution (>100 nm in $CHCl_3$) and solid state (>150 nm in film). Intramolecular charge transfer (ICT) properties of the synthesized compounds are examined using UV–Vis absorptions, photoluminescence measurements and solvatochromic studies. Our studies suggest that Stokes shifts of these compounds can be fine-tuned by manipulating the ICT strength between donor and acceptor with various electronic donating groups, and the largest Stokes shifts are typically associated with compounds that have the strong ICT characters. The observed spectroscopic properties of the compounds are consistent with theoretical calculations using density function theory (DFT) or time-dependent density function theory (TD-DFT). The calculations suggest that the ICT occurs from localized HOMO to localized LUMO with magnitudes of 60–80%. The relative quantum yields of these fluorophores in solution are various and highly solvent dependent. In solid state, the quantum yields of the compounds are significantly increased and some can reach to 0.40.

1. Introduction

Organic π-conjugated compounds have been extensively explored as the photonic-related materials in many disciplines of science due to their special photophysical properties of light absorption and emission. In this process, photons are absorbed and re-emitted, which results in the occurrence of energy relaxation from high energy wavelength to low energy wavelength. Therefore, these materials have wide applications including organic field-effect transistors [1], organic light-emitting diodes [2], organic photovoltaics [3–5] and biochemical sensors [6]. On the other hand, these π-conjugated compounds can also be used as wavelength-shifting materials to improve performance of cadmium telluride (CdTe) solar cells. It is known that CdTe solar cells have poor response efficiency (<20%) to the light under 500 nm. To improve the light response under 500 nm of the solar cells, a layer of wavelength-shifting materials, which absorb the light under 500 nm and re-emit light at more favorable wavelength (>550 nm), can be placed on the surface of the solar cells [7].

It is well known that anthracene [8], pyrene [9] and perylene [10] derivatives show high light-emitting performance due to their high quantum yields and have been widely used to develop new optical devices. However, small Stokes shifts (<25 nm) are typically associated with these types of materials, which can lead to serious self-quenching [11] and constrain the full potential of their applications. To enlarge the Stokes shift of these materials and eliminate the mentioned weakness in their applications, one possible solution is to create a Förster resonance energy transfer (FRET) system, which contains donor and acceptor molecules [12]. In this system, emission at a longer wavelength can be achieved by the emission of acceptor, which gets the excitation energy from the absorption of the donor at short wavelength – the pseudo Stokes shift is typically over 50 nm. However, this design requires a spectral overlap between the donor emission and the acceptor absorption as well as the adequate distance between them. More importantly, parallel alignment of the dipole moments of the donor and acceptor is required to reduce the energy loss caused by fluorescence anisotropy. To avoid these constrain associated with the FRET system, new approaches are needed to design new fluorophores with large Stokes shift and other optimal photophysical properties such as high quantum yields. It is found recently that compounds with strong intramolecular charge transfer (ICT) properties show large Stokes shifts based on the theory of Lippert and Mataga [13,14]. Large Stokes shift has been achieved in organic fluorophores

* Corresponding author. Tel.: +86 21 54747118.
** Corresponding author. Tel.: +1 509 335 5798.
E-mail addresses: thren@sjtu.edu.cn (T. Ren), wdong@vetmed.wsu.edu (W.-J. Dong).

1010-6030/$ – see front matter © 2012 Elsevier B.V. All rights reserved.
http://dx.doi.org/10.1016/j.jphotochem.2012.10.002

consisting of electron donating and accepting parts with the increase of conjugation bridge length [15]. However the intermolecular aggregation due to the long chains of these fluorophores can significantly reduce their energy conversion efficiency [16]. It has also noticed that stronger electron-withdrawing groups attached to the acceptor increase the ICT character of the fluorophore [17], therefore, different electron-withdrawing groups can be used to tuning the ICT character [18].

Here, we reported a study on tuning the ICT properties of a series of triphenylamine-based aromatic cyano compounds by manipulation the conjugation and strength of different donors and acceptors of the compounds. Strong ICT character (near 80% theoretically) accompanied by large Stokes shifts (over 100 nm in $CHCl_3$) and quantum yields up to 0.19 in $CHCl_3$ and 0.73 in 1,4-dioxane were observed with these synthesized red-emitting fluorophores. Properties of these compounds in solid state are also studied. The quantum yield in solid state is estimated up to 0.40. Potentially, these red-emitting fluorophores may find applications in wavelength-shifting materials for enhancement of the efficiency of some man-made solar cells.

2. Experimental

2.1. General methods

All reagents were used as received and without further purification. Chromatographic purification was carried out with 60-200 mesh silica gel for flash columns. Final compounds were characterized by ^{1}H NMR, ^{13}C NMR, MALDI-MS and elemental analysis (C, H, N percentage) to prove the purity for the spectroscopic measurements.

2.2. Spectroscopic measurements

Absorption spectra were recorded with a Bechman Coulter DU730 Life Science UV–Vis spectrophotometer at room temperature. Emission spectra from 200 nm to 800 nm were collected on an ISS PC1 photon counting spectrofluorometer at 20 °C. Fluorescence lifetimes were measured on a HORIBA JOBIN YVON fluorocube using 459 nm LED as the excitation light source.

2.3. Computational methods

All calculations were conducted by using the Gaussian 09 package [19].

2.4. Compounds characterization

2.4.1. 2-((4′-(Diphenylamino)biphenyl-4-yl)methylene)malononitrile (**1a**)

Red solid (yield 11%). R_f = 0.43 (Hex:EtOAc = 3:1). ^{1}H NMR (300 MHz, $CDCl_3$, δ): 7.97 (d, 2H, J = 8.5 Hz), 7.75 (s, 1H), 7.73 (d, 2H, J = 8.7 Hz), 7.54 (d, 2H, J = 8.8 Hz), 7.31 (t, 4H), 7.18-7.08 (m, 8H). ^{13}C NMR (75 MHz, $CDCl_3$, δ): 159.4, 149.2, 147.3, 147.0, 131.8, 131.7, 129.7, 129.4, 128.2, 127.3, 125.4, 124.0, 122.9, 114.4, 113.3, 81.2. MALDI-MS: m/z calcd for $C_{28}H_{19}N_3^+$ 397.1579, found 397.0719. Anal. (%): calcd (found) for $C_{28}H_{19}N_3$: C 84.61 (84.58), H 4.82 (4.18), N 10.57 (10.44).

2.4.2. 2-((4′-(Dip-tolylamino)biphenyl-4-yl)methylene)malononitrile (**1b**)

Red solid (yield 26%). R_f = 0.20 (Hex:EtOAc = 10:1). ^{1}H NMR (300 MHz, $CDCl_3$, δ): 7.95 (d, 2H, J = 8.5 Hz), 7.74 (s, 1H), 7.71 (d, 2H, J = 8.6 Hz), 7.49 (d, 2H, J = 8.9 Hz), 7.13-7.04 (m, 10H), 2.34 (s, 6H). ^{13}C NMR (75 MHz, $CDCl_3$, δ): 159.4, 149.6, 147.2, 144.7, 133.9, 131.8, 130.7, 130.3, 129.2, 128.0, 127.1, 125.6, 121.6, 114.5, 113.3, 80.9, 21.1. MALDI-MS: m/z calcd for $C_{30}H_{23}N_3^+$ 425.1892, found 425.2034. Anal. (%): calcd (found) for $C_{30}H_{23}N_3$: C 84.68 (84.25), H 5.45 (4.99), N 9.87 (9.78).

2.4.3. 2-((4′-(Bis(4-methoxyphenyl)amino)biphenyl-4-yl)methylene)malononitrile (**1c**)

Black solid (yield 14%). R_f = 0.31 (Hex:EtOAc = 3:1). ^{1}H NMR (300 MHz, $CDCl_3$, δ): 7.94 (d, 2H, J = 8.6 Hz), 7.73 (s, 1H), 7.70 (d, 2H, J = 8.6 Hz), 7.48 (d, 2H, J = 8.9 Hz), 7.11 (d, 4H, J = 9.0 Hz), 6.97 (d, 2H, J = 8.8 Hz), 6.87 (d, 4H, J = 9.0 Hz), 3.82 (s, 6H). ^{13}C NMR (75 MHz, $CDCl_3$, δ): 159.3, 156.7, 150.1, 147.2, 140.2, 131.8, 129.6, 129.0, 128.0, 127.5, 127.0, 119.7, 115.1, 114.5, 113.4, 80.7, 55.7. MALDI-MS: m/z calcd for $C_{30}H_{23}N_3O_2^+$ 457.1790, found 425.2006. Anal. (%): calcd (found) for $C_{30}H_{23}N_3O_2$: C 78.75 (78.63), H 5.07 (4.91), N 9.18 (8.91).

2.4.4. 2-((5-(4-(Diphenylamino)phenyl)thiophen-2-yl)methylene)malononitrile (**2a**)

Red solid (yield 19%). R_f = 0.31 (Hex:EtOAc = 3:1). ^{1}H NMR (300 MHz, $CDCl_3$, δ): 7.74 (s, 1H), 7.67 (d, 1H, J = 4.2 Hz), 7.53 (d, 2H, J = 8.7 Hz), 7.35-7.29 (m, 5H), 7.16-7.13 (m, 6H), 7.05 (d, 2H, J = 8.7 Hz). ^{13}C NMR (75 MHz, $CDCl_3$, δ): 157.4, 150.6, 150.1, 146.8, 140.7, 133.3, 129.8, 127.8, 125.7, 125.0, 124.6, 123.5, 121.9, 114.8, 114.0, 75.2. MALDI-MS: m/z calcd for $C_{26}H_{17}N_3S^+$ 403.1143, found 403.0908. Anal. (%): calcd (found) for $C_{26}H_{17}N_3S$: C 77.39 (76.79), H 4.25 (4.07), N 10.41 (10.14).

2.4.5. 2-((5-(4-(Dip-tolylamino)phenyl)thiophen-2-yl)methylene)malononitrile (**2b**)

Red solid (yield 20%). R_f = 0.35 (Hex:EtOAc = 5:1). ^{1}H NMR (300 MHz, $CDCl_3$, δ): 7.73 (s, 1H), 7.66 (d, 1H, J = 4.2 Hz), 7.49 (d, 2H, J = 9.0 Hz), 7.30 (d, 1H, J = 4.2 Hz), 7.12 (d, 4H, J = 8.2 Hz), 7.04 (d, 4H, J = 8.5 Hz), 6.97 (d, 2H, J = 8.9 Hz) 2.34 (s, 6H). ^{13}C NMR (75 MHz, $CDCl_3$, δ): 191.3, 157.8, 150.5, 144.2, 140.7, 134.4, 133.0, 130.4, 127.7, 125.9, 124.1, 123.2, 120.7, 114.9, 114.0, 74.8, 21.1. MALDI-MS: m/z calcd for $C_{28}H_{21}N_3S^+$ 431.1456, found 431.1379. Anal. (%): calcd (found) for $C_{28}H_{21}N_3S$: C 77.93 (77.09), H 4.90 (4.54), N 9.74 (9.67).

2.4.6. 2-((5-(4-(Bis(4-methoxyphenyl)amino)phenyl)thiophen-2-yl)methylene)malononitrile (**2c**)

Black solid (yield 22%). R_f = 0.24 (Hex:EtOAc = 3:1). ^{1}H NMR (300 MHz, $CDCl_3$, δ): 7.71 (s, 1H), 7.64 (d, 1H, J = 4.2 Hz), 7.42 (d, 2H, J = 8.8 Hz), 7.28 (d, 1H, J = 4.2 Hz), 7.10 (d, 4H, J = 8.9 Hz), 6.87 (d, 6H, J = 8.9 Hz), 3.82 (s, 6H). ^{13}C NMR (75 MHz, $CDCl_3$, δ): 158.0, 157.0, 151.0, 150.4, 140.9, 139.6, 132.8, 127.8, 127.7, 123.3, 123.0, 119.0, 115.2, 115.0, 114.1, 74.4, 55.7. MALDI-MS: m/z calcd for $C_{28}H_{21}N_3O_2S^+$ 463.1345, found 463.1473. Anal. (%): calcd (found) for $C_{28}H_{21}N_3O_2S$: C 72.55 (71.71), H 4.57 (4.33), N 9.06 (9.11).

2.4.7. 2-((5-(4-(Diphenylamino)phenyl)furan-2-yl)methylene)malononitrile (**3a**)

Red solid (yield 60%). R_f = 0.10 (Hex:EtOAc = 5:1). ^{1}H NMR (300 MHz, $CDCl_3$, δ): 7.69 (d, 2H, J = 9.0 Hz), 7.34-7.29 (m, 5H), 7.24-7.05 (m, 10H), 6.81 (d, 1H, J = 3.9 Hz). ^{13}C NMR (75 MHz, $CDCl_3$, δ): 189.8, 150.4, 147.0, 146.7, 140.6, 129.8, 127.2, 125.9, 124.7, 121.5, 120.7, 115.2, 114.2, 108.6, 73.3. MALDI-MS: m/z calcd for

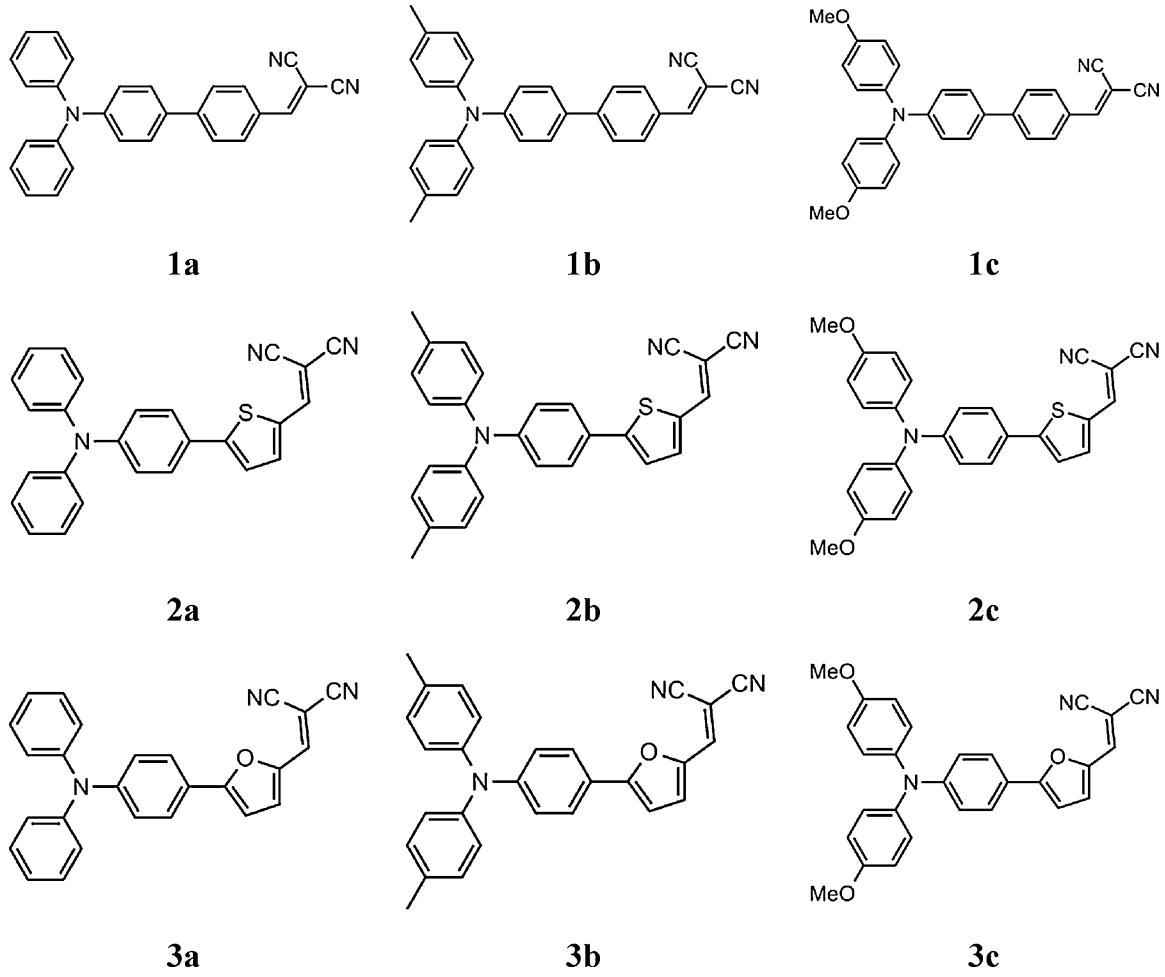

Fig. 1. Molecular structures of compounds **1a**–**3c**.

$C_{26}H_{17}N_3O^+$ 387.1372, found 387.1345. Anal. (%): calcd (found) for $C_{26}H_{17}N_3O$: C 80.60 (80.50), H 4.42 (4.21), N 10.85 (10.51).

2.4.8. 2-((5-(4-(Dip-tolylamino)phenyl)furan-2-yl)methylene)malononitrile (*3b*)

Red solid (yield 28%). R_f = 0.23 (Hex:EtOAc = 3:1). ^{1}H NMR (300 MHz, $CDCl_3$, δ): 7.65 (d, 2H, J = 8.9 Hz), 7.30 (s, 1H), 7.13 (d, 4H, J = 8.2 Hz), 7.06-6.99 (m, 7H), 6.78 (d, 1H, J = 3.9 Hz), 2.35 (s, 6H). ^{13}C NMR (75 MHz, $CDCl_3$, δ): 189.8, 162.6, 150.8, 146.9, 144.1, 134.6, 130.5, 130.2, 127.2, 126.1, 120.3, 119.7, 115.4, 114.3, 108.3, 72.8, 21.2. MALDI-MS: m/z calcd for $C_{28}H_{21}N_3O^+$ 415.1685, found 415.2174. Anal. (%): calcd (found) for $C_{28}H_{21}N_3O$: C 80.94 (80.96), H 5.09 (4.76), N 10.11 (10.47).

2.4.9. 2-((5-(4-(Bis(4-methoxyphenyl)amino)phenyl)furan-2-yl)methylene)malononitrile (*3c*)

Red solid (yield 86%). R_f = 0.73 (Hex:DCM = 1:3). ^{1}H NMR (300 MHz, $CDCl_3$, δ): 7.63 (d, 2H, J = 8.9 Hz), 7.25 (s, 1H), 7.19 (s, 1H), 7.10 (d, 4H, J = 9.0 Hz), 6.92-6.86 (m, 6H), 6.75 (d, 1H, J = 3.9 Hz), 3.81 (s, 6H). ^{13}C NMR (75 MHz, $CDCl_3$, δ): 189.8, 162.8, 157.2, 151.2, 146.8, 139.5, 127.9, 127.3, 127.0, 118.9, 118.6, 115.2, 115.0, 114.5, 108.2, 72.3, 55.8. MALDI-MS: m/z calcd for $C_{28}H_{21}N_3O_3^+$ 447.1583, found 447.2130. Anal. (%): calcd (found) for $C_{28}H_{21}N_3O_3$: C 75.15 (74.60), H 4.73 (4.64), N 9.39 (9.45).

3. Results and discussion

3.1. Molecular structures and synthesis

The molecular structures of triphenylamine-based aromatic cyano fluorophores **1a**–**3c** are depicted in Fig. 1 They were prepared by two steps from the corresponding *p*-substituted 4-bromotriphenylamine derivatives as illustrated in Scheme 1. The starting material **s-a** was commercially available while **s-b** and **s-c** were synthesized according to the Buchwald–Hartwig coupling [20], which is followed by Suzuki–Miyaura coupling to obtain product precursors **p-1a** to **p-3c** in good yields (70-95%) [21–26]. The final products **1a**–**3c** were synthesized from the reaction between the corresponding precursors and malononitrile by the Knoevenagel condensation. Compounds **1a**, **1b**, **2a** and **3a** have been reported before [27–29], but their photophysical properties have not been studied in detail yet.

3.2. Photophysical properties in chloroform solutions

Photophysical properties of these compounds were investigated by spectroscopic measurements. Fig. 2 shows their absorption and emission spectra in chloroform and the pertinent photophysical parameters are summarized in Table 1.

The structure of all fluorophores consists of two groups. One is triphenylamine (TPA) groups serving as electron donor (D) and the other is aromatic cyano groups as electron acceptor (A). In the

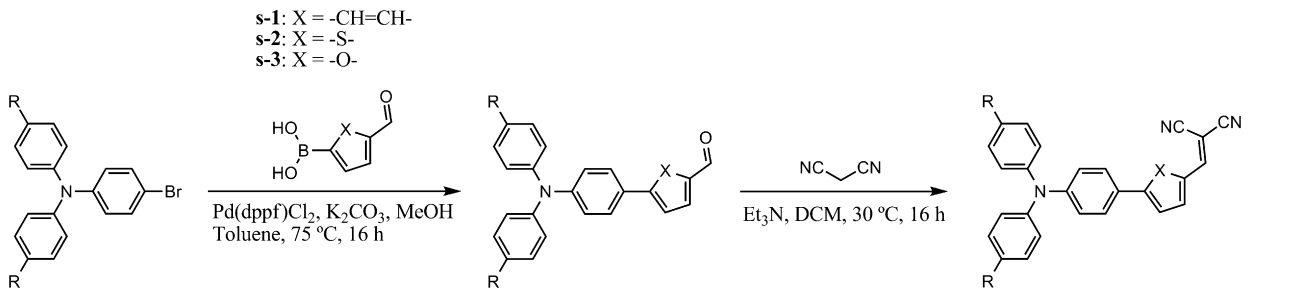

s-a: R = -H
s-b (59 %): R = -CH_3
s-c (66 %): R = -OCH_3

p-1a (70 %): R = -H, X = -CH=CH-
p-1b (79 %): R = -CH_3, X = -CH=CH-
p-1c (90 %): R = -OCH_3, X = -CH=CH-
p-2a (94 %): R = -H, X = -S-
p-2b (40 %): R = -CH_3, X = -S-
p-2c (95 %): R = -OCH_3, X = -S-
p-3a (75 %): R = -H, X = -O-
p-3b (76 %): R = -CH_3, X = -O-
p-3c (90 %): R = -OCH_3, X = -O-

1a (11 %): R = -H, X = -CH=CH-
1b (26 %): R = -CH_3, X = -CH=CH-
1c (14 %): R = -OCH_3, X = -CH=CH-
2a (19 %): R = -H, X = -S-
2b (20 %): R = -CH_3, X = -S-
2c (22 %): R = -OCH_3, X = -S-
3a (60 %): R = -H, X = -O-
3b (28 %): R = -CH_3, X = -O-
3c (86 %): R = -OCH_3, X = -O-

Scheme 1. Synthetic route of compounds **1a**–**3c**.

donor parts, methyl (**1b**, **2b** and **3b**) or methoxy (**1c**, **2c** and **3c**) group was introduced into the *para*-position of the TPA to increase the electron density on the donor. Similarly, electron density on the acceptor was enhanced by substituting the phenyl (**1a**–**c**) for thiophene (**2a**–**c**) or furan (**3a**–**c**) structure with the cyano groups. Since overall electronic distribution of molecule is closely related to the ICT property of the compound, combination of donors and acceptors with different electron densities generates fluorophores with various ICT strengths.

Our absorption and emission spectra results show that enhancement of overall electron density of whole conjugated molecule, which lowers the total energy of the molecular system, leads to red-shift in both absorption and emission spectra. All fluorophores show two groups of absorbance bands. The lower energy

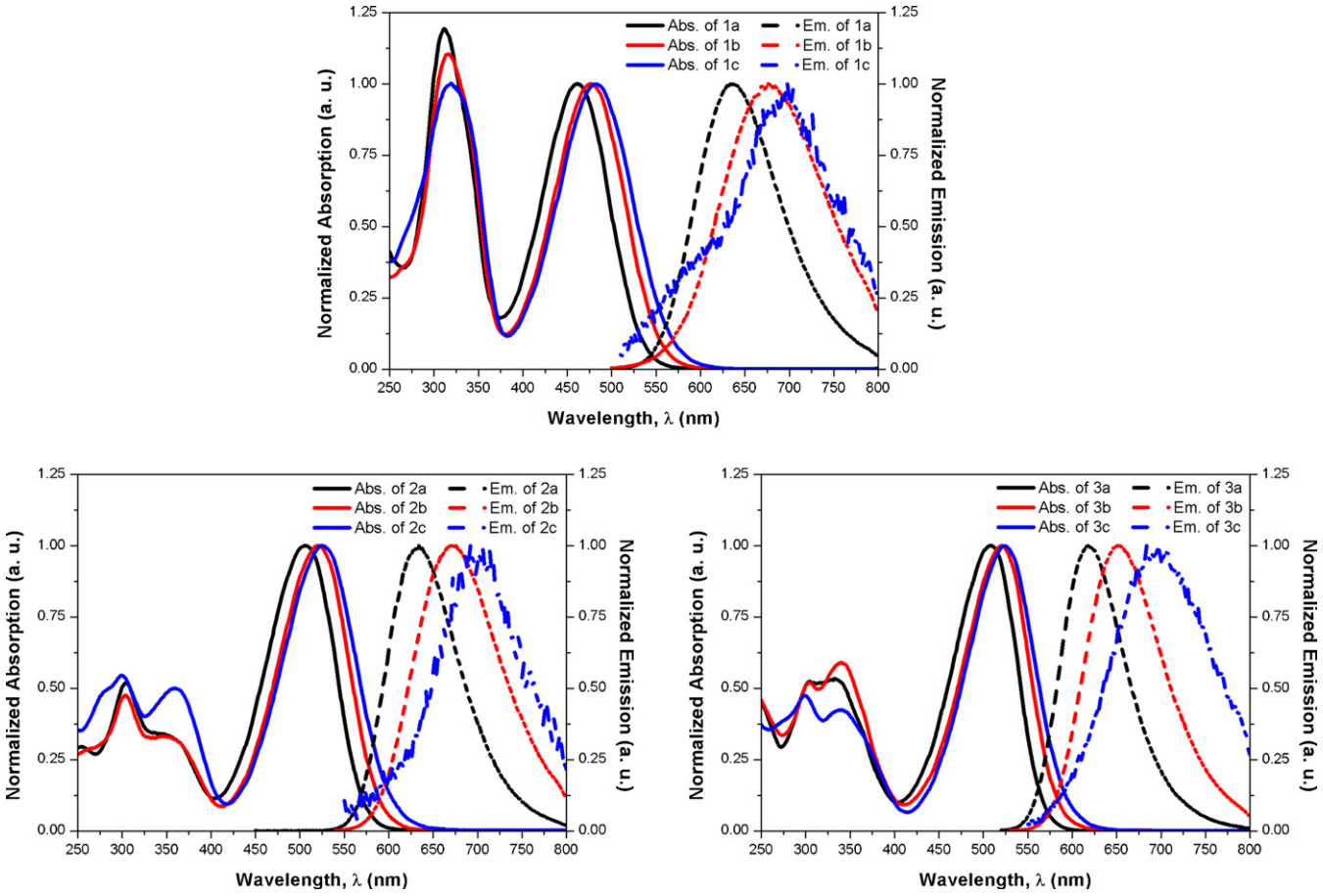

Fig. 2. Normalized UV–Vis absorption (solid lines) and photoluminescence (dashed lines) spectra in $CHCl_3$. Top: **1a** (λ_{ex} = 461 nm, black), **1b** (λ_{ex} = 477 nm, red), **1c** (λ_{ex} = 483 nm, blue). Left bottom: **2a** (λ_{ex} = 506 nm, black), **2b** (λ_{ex} = 521 nm, red), **2c** (λ_{ex} = 525 nm, blue). Right bottom: **3a** (λ_{ex} = 509 nm, black), **3b** (λ_{ex} = 521 nm, red), **3c** (λ_{ex} = 524 nm, blue). (For interpretation of the references to color in this figure legend, the reader is referred to the web version of the article.)

Table 1
Photophysical parameters of compounds **1a**–**3c** in chloroform including absorption maximum (λ_{abs}), molar absorption coefficient (ε) and emission (λ_{em}) maximum, Stokes shift ($\Delta\lambda = \lambda_{em} - \lambda_{abs}$), fluorescence quantum yield (Φ_f) and lifetime (τ_f), radiative (k_r) and nonradiative (k_{nr}) rate constants.

	λ_{abs} (nm)	ε (M^{-1} cm^{-1})	λ_{em} (nm)[a]	$\Delta\lambda$ (nm)	Φ_f[b]	τ_f (ns)	k_r (10^7 s^{-1})	k_{nr} ($10^7 s^{-1}$)
1a	312 461	35,655 29,894	634	173	0.19	3.64	5.21	22.25
1b	316 477	50,944 46,040	676	199	0.02	1.06	1.70	92.64
1c	319 483	37,414 37,271	696	213	<0.01	<1.00	–	–
2a	304 506	22,819 44,126	634	128	0.18	2.50	7.20	32.80
2b	303 521	16,987 35,641	670	151	0.07	2.17	3.04	43.04
2c	300 525	17,244 31,739	700	175	<0.01	<1.00	–	–
3a	305 509	20,914 36,532	618	109	0.19	2.73	6.96	29.67
3b	305 521	21,693 36,893	654	133	0.10	2.57	3.89	35.02
3c	300 524	17,034 40,071	696	172	<0.01	<1.00	–	–

[a] Excited at the lower energy of λ_{abs}.
[b] Excited at 470 nm. 4-Dimethylamino-4′-nitrostilbene as the standard (Φ_f = 0.70 in benzene).

absorbance bands (460-520 nm) are ascribed to the ICT process, while the higher energy absorbance bands (300-320 nm) are the π–π* or n–π* transitions on both donor and acceptor [31]. It is noted that the intensity of the electron transition absorbance band of compounds **2a**–**c** and **3a**–**c** are about half of that of compounds **1a**–**c** in their absorption spectra. This is probably due to the additional n–π* transition on the acceptor groups of **2a**–**c** (thiophene) and **3a**–**c** (furan), which suppresses the other electron transitions within the molecules. Therefore, there are two absorbance bands (300 nm and 350 nm) observed in the absorption spectra of **2a**–**c** and **3a**–**c** rather than only one band of **1a**–**c**. Furthermore, ICT enhanced red-shift in emission spectra was also observed. In the same solvent condition, the emission spectra show various shifts with changes of the ICT strength. Therefore, our results suggest that increasing ICT strength increases the Stokes shift of the fluorophores (e.g. **c** > **b** > **a**, or **3** > **2** > **1** in series).

In addition to fine-tune property of Stokes shift of the fluorophores by adjusting the D–A electron densities of the conjugated compounds, the fluorescence quantum yields of the fluorophores are also changed in response to changes of the D–A electron densities. For example, higher quantum yields ($\Phi_F \sim 20\%$) are observed with those molecules (**1a**, **2a** and **3a**) having weaker D–A interaction, and low fluorescence and short fluorescence lifetime are found to be associated with the fluorophores with methoxy group substituted TPA (**1c**, **2c** and **3c**), which have strongest ICT strength among the series.

3.3. Fluorescence solvatochromism

It is well known that ICT occurs upon the excitation of the fluorophores having D–A interactions. For a fluorophore with strong D–A interaction, this process is expected to be sensitive to environmental changes. To further characterize ICT and to understand the solvent relaxation mechanism of these synthesized compounds, fluorescence solvatochromism established by Jortner [32] and Reichardt [33] was performed (Figs. 3 and 4). Previous researches have shown that the emission spectra of the ICT fluorophores are expected to shift in response to the changes of the solvent polarity [34,35]. Herein, different mix ratios of 1,4-dioxane (DXE) and acetonitrile (ACN) were used to change solvent polarity and to examine the emission solvatochromatic shift of **3a**. The result is depicted in Fig. 3. Obviously, with the increase of the relative solvent polarity (water as standard for the polarity of 1.000) from 0.164 (1,4-dioxane) to 0.460 (acetonitrile), the emission maximum shifts from 580 nm to 676 nm. The decrease of the emission energy is mainly caused by the solvent relaxation process, which is a strong dipole–dipole interaction between the fluorophore in its excited state and the surrounding solvent molecules. As a consequence, a portion of the absorbed energy is consumed for the solute–solvent (λ_s) and intramolecular (λ_i) reorganization energies [36].

More precisely, the solvent relaxation process of the ICT fluorophore can be described by the Lippert–Mataga equation.

$$(\nu_{abs}^{ICT} - \nu_{flu}^{ICT}) = (\nu_{abs}^{vac} - \nu_{flu}^{vac}) + \frac{2(\mu_e - \mu_g)^2}{hca_0^3}\Delta f$$

$$\Delta f = \frac{\varepsilon - 1}{2\varepsilon + 1} - \frac{n^2 - 1}{2n^2 + 1}$$

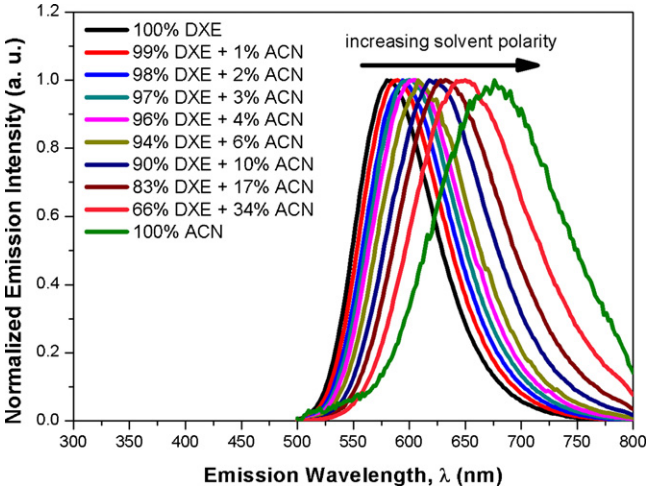

Fig. 3. Solvatochromatic shift of **3a** in different DXE/ACN mixtures.

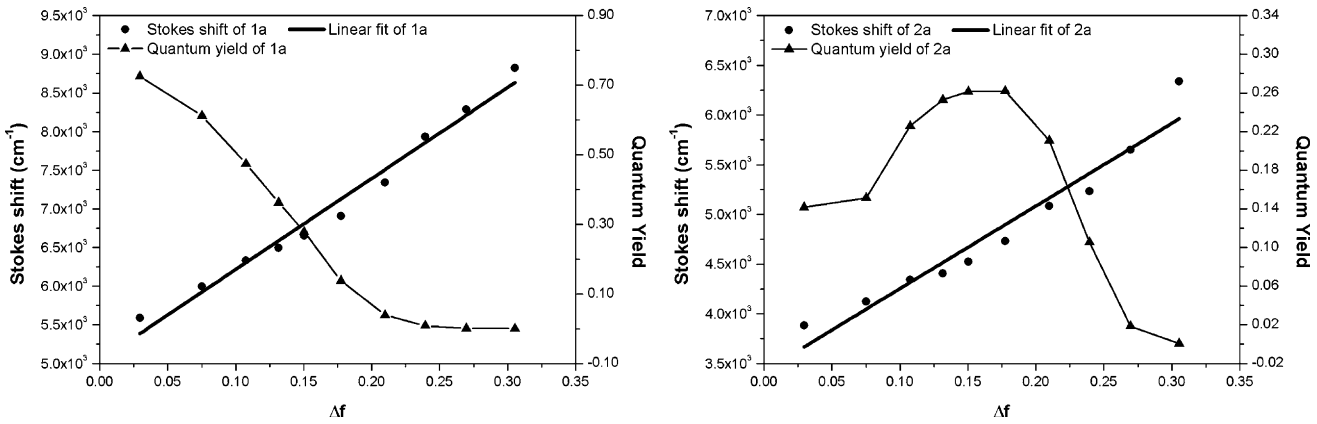

Fig. 4. Solvatochromatic shift and quantum yield change of **1a** (left) and **2a** (right).

where ν is the wavenumber (cm^{-1}); the superscript ICT and vac mean ICT state and gas state, respectively; the subscript abs and flu mean absorption and emission process, respectively; μ_e and μ_g are dipole moment (1D = 10^{-18} esu cm) of the excited and ground state, respectively; h is the Planck's constant 6.63×10^{-27} (erg s); c is the speed of light 3×10^{10} (cm s^{-1}); a_0 (cm) is the cavity radius of Onsagar's reaction field, which is approximate to 40% of the longest axis for nonspherical molecules of their ground state geometries [37]. Δf is defined as orientation polarizability and can be tuned by mixtures of 1,4-dioxane and acetonitrile solutions. The corresponding dielectric constant (ε) and refractive index (n) of the solvent mixture were calculated using the following equation.

$$\varepsilon = \chi_{DXE}\varepsilon_{DXE} + \chi_{ACN}\varepsilon_{ACN}$$

$$n = \sqrt{\chi_{DXE}n_{DXE}^2 + \chi_{ACN}n_{DXE}^2}$$

Fig. 4 shows linear relationship of Stoke shifts of compounds **1a** and **2a** to the changes of the orientation polarizability, Δf. Also shown in Fig. 4 are changes in fluorescence quantum yields of fluorophores **1a** and **2a** to the changes of Δf (the results for other compounds are shown in Figs. 4 and 5 in Supplementary data).

As expected, all compounds show increased Stokes shift along with increase of Δf, suggesting that they are all strong ICT fluorophores with highly localized excited state charge separation. The slopes of the linear relationship between Stoke shifts and changes in Δf shown in Fig. 4 are 11,764 for fluorophore **1a** and 8318 for fluorophore **2a**, respectively. The steeper slope obtained with **1a** indicates that fluorophore **1a** undergoes a larger dipole change ($\mu_e - \mu_g$) during the excitation than that of fluorophore **2a**. Similarly, due to the decrease of the D–A interaction in the molecules, compounds **1c**, **2c** and **3c** show weakest ICT strength (Table 2 in Supplementary data).

Unlike the changes of Stokes shift, the changes of the quantum yield are quite different for each compound. Quantum yield of compound **1a** changes from 0.19 in chloroform to 0.73 in 1,4-dioxane (Fig. 4) because Δf of 1,4-dioxane (0.131) is a half of the Δf of chloroform (0.254). Quantum yield of compound **1a** exhibits a trend of decrease in quantum yield with the increase of Δf. Similar results were obtained from compound **1b** (Fig. 5 in Supplementary data). Generally speaking, with the increase of the solvent orientation polarizability (Δf), it will take more time for a typical ICT fluorophore to reach the relaxed state from its excited state in solution, which enhances the non-radiative process and leads to more energy loss to the surrounding solvent dipole changes. Therefore, the quantum yield is expected to decrease. However, for fluorophore **2a**, the quantum yield changes in two-phase, it first increases and then decreases after $\Delta f = 0.18$, which is approximate 6-10% acetonitrile in 1,4-dioxane solution. Similar changes are found in fluorophore **3a** (Fig. 5 in Supplementary data). The mechanism of this two-phase change in quantum yield is unknown. Since the excitation coefficient and radiative decay rates are usually not very sensitive to solvent polarity [38], the increasing phase of **2a** and **3a** may suggest different response of non-radiative processes of these fluorophores to different solvent polarities.

3.4. Theoretical studies

To further understand the properties of the ground and excited states of the synthesized fluorophores, we performed quantum chemistry computation on all the compounds. Ground state (S_0) geometry optimizations were first performed at the B3LYP/6-311G(d, p) level of DFT theory without symmetry constraint. Excited state (S_1) geometries were obtained by the TD method with the same function. It should be point out that all the calculations were processed without using the SCRF (Self-Consistent Reaction Field) method to reduce the computational efforts. Thus, the output results represent the gas state properties of all the fluorophores. The calculated results and proposed absorption and emission process mechanism are depicted in Table 2 and Fig. 5 (only **1b** was shown as example), respectively (results for all other compounds are given in Tables 3 and 4 in Supplementary data). Table 2 shows the energy of highest occupied molecular orbital (HOMO) and lowest unoccupied molecular orbital (LUMO) as well as the charge separation percentages of donor (D) or acceptor (A) and their related ICT characters during the excitation process. As expected, the computationally

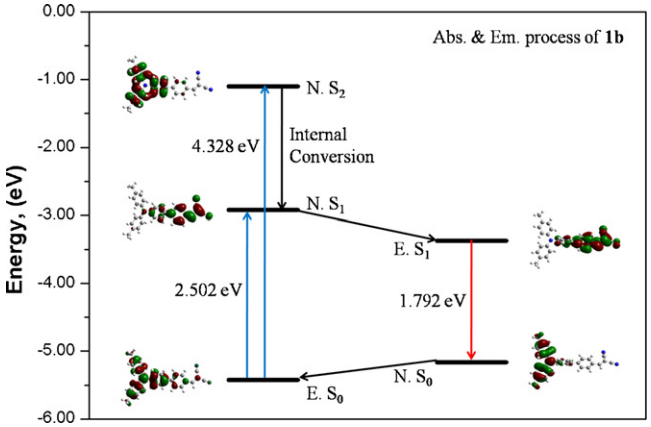

Fig. 5. Mechanism of absorption and emission process of **1b** (E. stands for equilibrium and N. stands for non-equilibrium).

Table 2
Theoretical calculations on HOMO and LUMO energy, charge separation percentage (%) of donor (D) or acceptor (A), the ICT character and geometric difference between the ground and excited states.

	HOMO			LUMO			ICT character
	eV	D	A	eV	D	A	
1a	−5.562	91%	9%	−2.977	11%	89%	80%
1b	−5.425	91%	9%	−2.923	11%	89%	80%
1c	−5.263	92%	8%	−2.861	11%	89%	81%
2a	−5.576	81%	19%	−2.965	16%	84%	65%
2b	−5.447	82%	18%	−2.906	16%	84%	66%
2c	−5.298	84%	16%	−2.844	16%	84%	68%
3a	−5.485	78%	22%	−2.856	14%	86%	64%
3b	−5.362	80%	20%	−2.795	16%	84%	64%
3c	−5.215	83%	17%	−2.725	16%	84%	67%

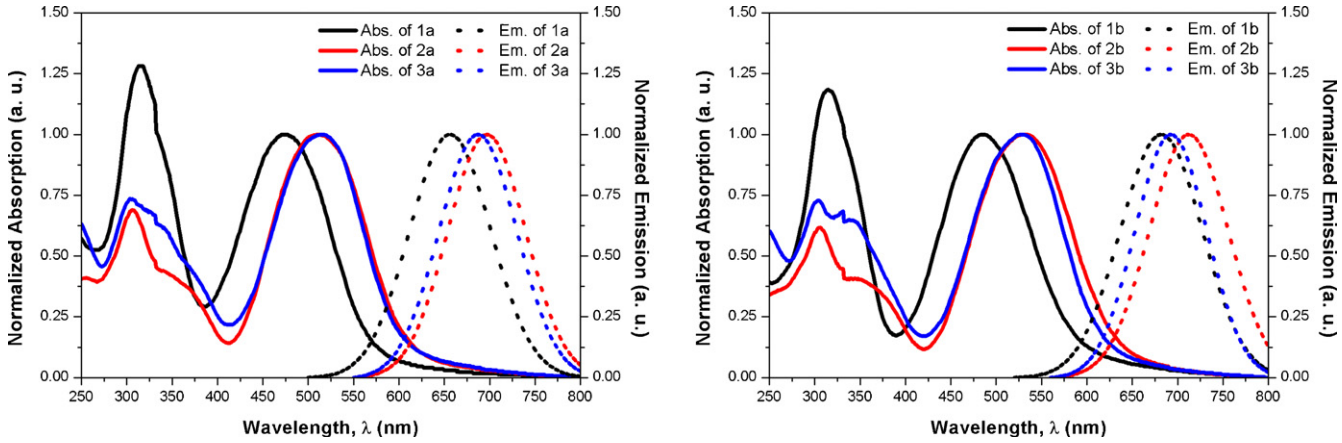

Fig. 6. Solid state absorption (solid lines) and emission (dashed lines) spectra. Left: **1a** (λ_{ex} = 476 nm, black), **2a** (λ_{ex} = 511 nm, red), **3a** (λ_{ex} = 516 nm, blue). Right: **1b** (λ_{ex} = 485 nm, black), **2b** (λ_{ex} = 531 nm, red), **3b** (λ_{ex} = 528 nm, blue). (For interpretation of the references to color in this figure legend, the reader is referred to the web version of the article.)

calculated ICT strengths are well consistent with the experimentally measured Stokes shifts, suggesting that all compounds are typical ICT fluorophores. Also, LUMO is highly localized with more than 80% charges on the acceptor moiety in the excited state of the fluorophore, which is consistent with the experimental results from the fluorescence solvatochromatic measurements. The slope increased by the increasing D–A interaction (or ICT strength) is consistent with the calculated ICT characters (Table 2 in Supplementary data).

It is illustrated in Fig. 5 that the ICT (E. $S_0 \rightarrow$ N. S_1) and π–π^* (E. $S_0 \rightarrow$ N. S_2) transitions occur from the equilibrium ground state to the non-equilibrium excited state with the energy gap of 2.502 eV and 4.328 eV, respectively, during the absorption process of **1b**. These calculated results are well consistent with the two absorbance bands found in the experimental absorption spectrum of **1b**. Furthermore, it is noted that a charge localized excited state (E. S_1) has also been found from the calculation, which explains the ICT properties observed from the florescence solvatochromatic measurement of **1b**. Same results are also found for the other fluorophores. During the emission process, charge transfers back from the equilibrium excited state (E. S_1) to the non-equilibrium ground state (N. S_0). The theoretical absorption and emission energies at

Table 3
Photophysical parameters of compounds **1a**–**b**, **2a**–**b** and **3a**–**b** in solid state including absorption (λ_{abs}), emission (λ_{em}) maximum and Stokes shift ($\Delta\lambda = \lambda_{em} - \lambda_{abs}$), compared with the data in chloroform (CLF) solution.

#	λ_{abs} (nm) (in CLF)	λ_{em} (nm) (in CLF)	$\Delta\lambda$ (nm) (in CLF)	$\Phi_{f,s}$ [a]
1a	316 (312) 476 (461)	658 (634)	182 (173)	0.40
2a	306 (304) 511 (506)	696 (634)	185 (128)	0.35
3a	304 (305) 516 (509)	686 (618)	170 (109)	0.36
1b	315 (316) 485 (477)	681 (676)	196 (199)	0.19
2b	306 (303) 531 (521)	713 (670)	182 (151)	0.15
3b	304 (305) 528 (521)	693 (654)	165 (133)	0.15

[a] Estimated solid state quantum yield. Quantum yield of compound **1a** was measured by using perylene (λ_{em} = 435 nm, $\Phi_{f,s}$ = 0.94) as standard, and the relative quantum yields of all other compounds were calculated by comparing with compound **1a**.

the gas state of all the fluorophores are calculated using bandgap analysis. For example, the calculated absorption and emission energy of compound **1b** are 2.502 eV (20,180 cm^{-1}) and 1.792 eV (14,454 cm^{-1}), respectively (Fig. 5). The calculated results for all other compounds are given in Supplementary data. These results are well correlated with the experimental results derived from the Lippert–Mataga equation (Table 2 in Supplementary data).

3.5. Photophysical properties in the solid state

To explore the applications using these fluorophores as wavelength-shifting materials, it is important to know the solid state photophysical properties of the fluorophores. The measured absorption and emission spectra in solid state are shown in Fig. 6. The absorption and emission parameters are summarized in Table 3.

The solid state absorption and emission spectra of **1c**, **2c** and **3c** were not measured due to their low fluorescent intensity. All other fluorophores emitted red light (over 650 nm) and showed a red-shift in emission spectra comparing to the spectra obtained from chloroform solution. The observed larger red-shifts in solid state comparing to solution samples may be resulted from the restrictive internal rotation (RIR) in the solid state, in which the fluorophore is restricted to reach its favorable electronic and geometric structure during the emission process and thus reduce the energy bandgap between the ground (N. S_0) and excited (E. S_1) states [40]. The ICT absorption maximum displays a red-shift behavior, revealing the main RIR effect that reduces the total energy gap may play important role in the molecular rotation between the donor and acceptor. Moreover, even though the absolutely quantum yields of the fluorophores in their solid state were not determined due to our instrumental limitation and the difficulties to find a solid state standard, the approximate quantum yield are estimated using perylene as standard (Table 3) (Section 4 in Supplementary data). Our measurements show that the relative quantum yields of all fluorophores, except **1c**, **2c** and **3c**, are significantly higher than that in their chloroform solution, especially, Compounds **1a**, **2a** and **3a** show quantum yields over 0.35. This indicates that the RIR effect in the solid state suppresses part of the energy relaxation caused by the internal rotation (IR) and increases emission quantum yields.

4. Conclusion

In conclusion, a series of triphenylamine-based aromatic cyano fluorophores have been synthesized. These fluorophores exhibit large Stokes shifts in solution (>100 nm in $CHCl_3$) and solid state (>150 nm in film) with a broad absorbance bands from UV region to 550 nm and a strong fluorescence peak various from 600 nm to 700 nm. Examination of the photophysical properties of these fluorophores suggests that TPA derivatives serve as donor and aromatic cyano as acceptor in these compounds. Fluorescence solvatochromatic studies are performed to understand solvent relaxation mechanism of these fluorophores. The results suggest red shifts in emission spectra of these compound are due to the increase in strength of the electron-donating group on the donor moiety (e.g. emission maximum: **1a** < **1b** < **1c**), which is consistent with ICT mechanism. Our study also suggest that dipole moment changes between donor and acceptor from the ground state to the excited state can also affect Stoke shifts of the fluorophores (e.g. **1a** > **2a** > **3a**). DFT and TD-DFT calculations reveal potential mechanism to support these results by showing that strong ICT (over 60%) occurs from localized HOMO (mainly on donor moiety) to localized LUMO (mainly on acceptor moiety). Solid state fluorescence measurements show that some of the fluorophores have high solid state quantum yield as well as large Stokes shifts, which may be due to the RIR effect to suppress energy relaxation process caused by the internal rotation (IR) of the molecule. These results provide insight information for fine-tuning the design of new wavelength-shifting compounds in the future.

Appendix A. Supplementary data

Supplementary data associated with this article can be found, in the online version, at http://dx.doi.org/10.1016/j.jphotochem.2012.10.002.

References

[1] Y. Song, C. Di, X. Yang, S. Li, W. Xu, Y. Liu, L. Yang, Z. Shuai, D. Zhang, D. Zhu, A cyclic triphenylamine dimer for organic field-effect transistors with high performance, Journal of the American Chemical Society 128 (2006) 15940–15941.
[2] A.C. Grimsdale, K.L. Chan, R.E. Martin, P.G. Jokisz, A.B. Holmes, Synthesis of light-emitting conjugated polymers for applications in electroluminescent devices, Chemical Reviews 109 (2009) 897–1091.
[3] Y.J. Cheng, S.H. Yang, C.S. Hsu, Synthesis of conjugated polymers for organic solar cell applications, Chemical Reviews 109 (2009) 5868–5923.
[4] P. Heremans, D. Cheyns, B.P. Rand, Strategies for increasing the efficiency of heterojunction organic solar cells: material selection and device architecture, Accounts of Chemical Research 42 (2009) 1740–1747.
[5] N. Martin, L. Sanchez, M.A. Herranz, B. Illescas, D.M. Guldi, Electronic communication in tetrathiafulvalene (TTF)/C60 systems: toward molecular solar energy conversion materials? Accounts of Chemical Research 40 (2007) 1015–1024.
[6] S.W. Thomas 3rd, G.D. Joly, T.M. Swager, Chemical sensors based on amplifying fluorescent conjugated polymers, Chemical Reviews 107 (2007) 1339–1386.
[7] L. Danos, T. Parel, T. Markvart, V. Barrioz, W.S.M. Brooks, S.J.C. Irvine, Increased efficiencies on CdTe solar cells via luminescence down-shifting with excitation energy transfer between dyes, Solar Energy Materials and Solar Cells 98 (2012) 486–490.
[8] H. Ihmels, A. Meiswinkel, C.J. Mohrschladt, Novel fluorescence probes based on 2,6-donor–acceptor–substituted anthracene derivatives, Organic Letters 2 (2000) 2865–2867.
[9] K. Fujimoto, H. Shimizu, M. Furusyo, S. Akiyama, M. Ishida, U. Furukawa, T. Yokoo, M. Inouye, Photophysical properties of 1,3,6,8-tetrakis(arylethynyl)pyrenes with donor or acceptor substituents: their fluorescence solvatochromism and lightfastness, Tetrahedron 65 (2009) 9357–9361.
[10] Y. Avlasevich, C. Kohl, K. Mullen, Facile synthesis of terrylene and its isomer benzoindenoperylene, Journal of Materials Chemistry 16 (2006) 1053–1057.
[11] X. Zhang, Y. Xiao, X. Qian, A ratiometric fluorescent probe based on FRET for imaging Hg^{2+} ions in living cells, Angewandte Chemie International Edition in English 47 (2008) 8025–8029.
[12] M. Suresh, S. Mishra, S.K. Mishra, E. Suresh, A.K. Mandal, A. Shrivastav, A. Das, Resonance energy transfer approach and a new ratiometric probe for Hg^{2+} in aqueous media and living organism, Organic Letters 11 (2009) 2740–2743.
[13] Z.R. Grabowski, K. Rotkiewicz, W. Rettig, Structural changes accompanying intramolecular electron transfer: focus on twisted intramolecular charge-transfer states and structures, Chemical Reviews 103 (2003) 3899–4032.
[14] F.B. Dias, S. Pollock, G. Hedley, L.O. Palsson, A. Monkman, I.I. Perepichka, I.F. Perepichka, M. Tavasli, M.R. Bryce, Intramolecular charge transfer assisted by conformational changes in the excited state of fluorene-dibenzothiophene-S,S-dioxide co-oligomers, Journal of Physical Chemistry B 110 (2006) 19329–19339.
[15] D.P. Hagberg, T. Marinado, K.M. Karlsson, K. Nonomura, P. Qin, G. Boschloo, T. Brinck, A. Hagfeldt, L. Sun, Tuning the HOMO and LUMO energy levels of organic chromophores for dye sensitized solar cells, Journal of Organic Chemistry 72 (2007) 9550–9556.
[16] P. Qin, X.C. Yang, R.K. Chen, L.C. Sun, T. Marinado, T. Edvinsson, G. Boschloo, A. Hagfeldt, Influence of pi-conjugation units in organic dyes for dye-sensitized solar cells, Journal of Physical Chemistry C 111 (2007) 1853–1860.
[17] S. Roquet, A. Cravino, P. Leriche, O. Aleveque, P. Frere, J. Roncali, Triphenylamine–thienylenevinylene hybrid systems with internal charge transfer as donor materials for heterojunction solar cells, Journal of the American Chemical Society 128 (2006) 3459–3466.
[18] P. Leriche, P. Frere, A. Cravino, O. Aleveque, J. Roncali, Molecular engineering of the internal charge transfer in thiophene–triphenylamine hybrid pi-conjugated systems, Journal of Organic Chemistry 72 (2007) 8332–8336.
[19] M.J. Frisch, G.W. Trucks, H.B. Schlegel, G.E. Scuseria, M.A. Robb, J.R. Cheeseman, G. Scalmani, V. Barone, B. Mennucci, G.A. Petersson, H. Nakatsuji, M. Caricato, X. Li, H.P. Hratchian, A.F. Izmaylov, J. Bloino, G. Zheng, J.L. Sonnenberg, M. Hada, M. Ehara, K. Toyota, R. Fukuda, J. Hasegawa, M. Ishida, T. Nakajima, Y. Honda, O. Kitao, H. Nakai, T. Vreven, J.A. Montgomery Jr., J.E. Peralta, F. Ogliaro, M. Bearpark, J.J. Heyd, E. Brothers, K.N. Kudin, V.N. Staroverov, R. Kobayashi, J. Normand, K. Raghavachari, A. Rendell, J.C. Burant, S.S. Iyengar, J. Tomasi, M. Cossi, N. Rega, J.M. Millam, M. Klene, J.E. Knox, J.B. Cross, V. Bakken, C. Adamo, J. Jaramillo, R. Gomperts, R.E. Stratmann, O. Yazyev, A.J. Austin, R. Cammi, C. Pomelli, J.W. Ochterski, R.L. Martin, K. Morokuma, V.G. Zakrzewski, G.A. Voth,

P. Salvador, J.J. Dannenberg, S. Dapprich, A.D. Daniels, O. Farkas, J.B. Foresman, J.V. Ortiz, J. Cioslowski, D.J. Fox, Gaussian 09, Revision A.01, Gaussian, Inc., Wallingford, CT, 2009.
[20] Y.J. Chang, T.J. Chow, Triaryl linked donor acceptor dyads for high-performance dye-sensitized solar cells, Tetrahedron 65 (2009) 9626–9632.
[21] C. Liu, Q.J. Ni, J.S. Qiu, Very fast, ligand-free and aerobic protocol for the synthesis of 4-aryl-substituted triphenylamine derivatives, European Journal of Organic Chemistry (2011) 3009–3015.
[22] Patent: JP11174701A.
[23] D.J. Schipper, K. Fagnou, Direct arylation as a synthetic tool for the synthesis of thiophene-based organic electronic materials, Chemistry of Materials 23 (2011) 1594–1600.
[24] Patent: JP2009093909A.
[25] Q.Y. Yu, J.Y. Liao, S.M. Zhou, Y. Shen, J.M. Liu, D.B. Kuang, C.Y. Su, Effect of hydrocarbon chain length of disubstituted triphenyl-amine-based organic dyes on dye-sensitized solar cells, Journal of Physical Chemistry C 115 (2011) 22002–22008.
[26] J.T. Lin, P.C. Chen, Y.S. Yen, Y.C. Hsu, H.H. Chou, M.C. Yeh, Organic dyes containing furan moiety for high-performance dye-sensitized solar cells, Organic Letters 11 (2009) 97–100.
[27] M. Ouyang, W.Q. Xiang, Y.J. Zhang, Y.X. Jin, C. Zhang, Synthesis, characterization and properties of electron donor–acceptor complexes based on 9,9-diarylfluorene, Acta Physico-Chimica Sinica 27 (2011) 1516–1524.
[28] Patent: JP2001064640A.
[29] C. Sissa, V. Parthasarathy, D. Drouin-Kucma, M.H. Werts, M. Blanchard-Desce, F. Terenziani, The effectiveness of essential-state models in the description of optical properties of branched push–pull chromophores, Physical Chemistry Chemical Physics 12 (2010) 11715–11727.
[31] J. Svoboda, P. Stenclova, F. Uhlik, J. Zednik, J. Vohlidal, Synthesis and photophysical properties of alpha,omega-bis(terpyridine)oligothiophenes, Tetrahedron 67 (2011) 75–79.
[32] B. Pullman, J. Jortner, Intramolecular dynamics, in: Proceedings of the 15th Jerusalem Symposium, Israel, 1982, vol. 15, D. Reidel Publishing Company, Dordrecht, Holland, 1982.
[33] C. Reichardt, Solvents and Solvent Effects in Organic Chemistry, Wiley-VCH, Weinheim, 1988 (2nd ed.), 2003 (3rd ed.).
[34] K.C. Moss, K.N. Bourdakos, V. Bhalla, K.T. Kamtekar, M.R. Bryce, M.A. Fox, H.L. Vaughan, F.B. Dias, A.P. Monkman, Tuning the intramolecular charge transfer emission from deep blue to green in ambipolar systems based on dibenzothiophene S,S-dioxide by manipulation of conjugation and strength of the electron donor units, Journal of Organic Chemistry 75 (2010) 6771–6781.
[35] G.L. Fu, H.Y. Zhang, Y.Q. Yan, C.H. Zhao, p-Quaterphenyls laterally substituted with a dimesitylboryl group: a promising class of solid-state blue emitters, Journal of Organic Chemistry 77 (2012) 1983–1990.
[36] J. Herbich, A. Kapturkiewicz, Electronic structure and molecular conformation in the excited charge transfer singlet-states of 9-acridyl and other aryl derivatives of aromatic amines, Journal of the American Chemical Society 120 (1998) 1014–1029.
[37] H. El-Gezawy, W. Rettig, R. Lapouyade, Solvatochromic behavior of donor–acceptor-polyenes: dimethylamino-cyano-diphenylbutadiene, Journal of Physical Chemistry A 110 (2006) 67–75.
[38] J.R. Lakowicz, Principles of Fluorescence Spectroscopy, 3rd ed., Springer Science+Business Media, NY, USA, 2006.
[40] Y. Hong, J.W. Lam, B.Z. Tang, Aggregation-induced emission, Chemical Society Reviews 40 (2011) 5361–5388.